RECYCLED AGGREGATE CONCRETE-FILLED STEEL COLUMN CONVEX DEFORMATION DETECTION VIA NON-CONTACT MEASUREMENT

Yunchao TANG[1], Lijuan LI[2]*, Wenxian FENG[3]*,Chenglin Wang[4], Xiangjun ZOU[5], Weiming SITU[6]

This paper presents a non-contact measurement technology in detecting convex deformation of Recycled aggregate concrete-filled steel columns (RACSCs). This novel measurement method was developed as an approximation of the traditional (contact) measurement method. The setup is comprised of a single camera and a laser range finder that establish a spatial-geometric relationship between the two tools and the convex deformation surface of the RACSC. An OpenCV-based visual detection system acquires an image of the convex deformation after the RACSC yields in a dynamic loading test. The edge of the convex deformation surface is measured with an improved Canny algorithm, then the noise is removed with a novel dual-gray-value assignment technique. The maximum diameter and height of the convex deformation of the RACSC are calculated by applying a Circle Hough Transform to the edge curve of convex deformation. We conducted a series of experiments to validate the proposed method and found that according to the images, convex deformation in the dynamic loading test appeared at the bottom of specimens and was uneven among the thin-walled RAC components. The average relative error of the maximum diameter of convex deformation between the proposed measurement method and the traditional measurement method was 3.15%, suggesting that the detection accuracy of the proposed method is reasonable.

Keywords: Monocular vision; Multi-sensor measurement; Three dimensional; Convex deformation; Canny algorithm

1. Introduction

Large span and heavy loading capacity are a new tide for modern bridge and engineering structure, and its key components, recycled aggregate

[1] School of Civil and Transportation Engineering, Guangdong University of Technology, Guangzhou 510006, China
[2] *(Corresponding author) School of Civil and Transportation Engineering, Guangdong University of Technology, Guangzhou 510006, China; Email: lilj@gdut.edu.cn
[3] *(Corresponding author) School of Civil and Transportation Engineering, Guangdong University of Technology, Guangzhou 510006, China; Email: fengwx@gdut.edu.cn
[4] Colleges of Engineering, South China Agricultural University, Guangzhou 510642, China
[5] Colleges of Engineering, South China Agricultural University, Guangzhou 510642, China
[6] Colleges of Engineering, South China Agricultural University, Guangzhou 510642, China

concrete-filled steel columns (RACSCs), have the substantial advantage for withstanding the harsh conditions. RACSCs subjected to shock force typically produce convex deformation, followed by cracking and rapid expansion when the seismic force exerted upon them exceeds their load capacity; of course, this represents a severe risk inherent to urban construction projects [1-3]. Catastrophes of this nature can be predicted to some extent in advance, however. The seismic performance of RACSC can be evaluated via early detection of the convex deformation [4]. Thus, this deformation induced by seismic force has drawn the scholars' a great deal of attention [5-8]. The deformation phenomena and seismic performance are studied via low cyclic load test used for seismic load simulation [9-11]. In the tests, the stress and displacement are measured by contact-type sensors [12]; the detection accuracy is rather limited as the sensors are pre-distributed in the expected area, while the crack and deformation is unpredictable to some extent due to the nonlinear behavior of the RACSC [7]. After the seismic test, the crack and deformation is manually measured, unfortunately. Traditional contact-type measurement of material strain or displacement is done using contact sensors like strain gauges. Accurate measurement of RACSC damage and deformation is the crux of engineering structural tests [7], and at present, most measurement techniques are contact-type and artificial. These tests are time consuming, prone to error, and laborious as they require manually painting lines on the surface of the deformation region. There are numerous application limitations as well as substantial risk in taking measurements for the convex deformation of RACSCs in bridges at high altitude [12]. Non-contact visual deformation detection can potentially mitigate these disadvantages while effectively facilitating the monitoring and evaluation of seismic structural damage [13-15]. To ensure the safety and the serviceability of civil infrastructure it is essential to visually inspect and assess its physical and functional condition [5].

Vision system-based measurement of convex deformation and crack parameters of RAC steel column currently is a relatively new concept, though there have been numerous valuable contributions to the literature in recent years. Binocular vision technology-based systems are mainly used for crack detection in concrete components; Xiao et al., for example, used image processing technology to study the cross-section fatigue failure of the recycled concrete specimens [13]. A stereovision-based crack width detection approach was developed for concrete surface assessment in another study [14]. An image-based retrieval method of concrete crack properties was proposed for bridge inspection [16-18]. Unfortunately, these systems tend to be too high in cost to be practically applicable [19]. Belen Ferrer developed a target less image-based method for measuring displacements and strains on concrete surfaces with a consumer camera [19]. Researcher established3D (three dimensional) position estimation of a

mobile robot with monocular vision [20]. Other researchers established an image processing technology-based method to detect cracks in concrete bridges with a relative error less than 10% [21]. Based on laser measurement technology, the interrupted layer in road engineering projects can be measured accurately [22]. When the visual depth distance of a target can be determined by the laser rangefinder, 3D information of the target can be obtained using image processing technology and geometric computing, though this is effectively limited to monocular vision. This method has important significance in regard to surface edge detection and damage assessment [23-24]. Though previous researches have focused mainly on the plane cracks, more complex surfaces in the building structure merit further research. To this effect, studies on the edge detection of complex curved surfaces have a great deal of practical significance.

Convex deformation edge detection theories and algorithms have been extensively researched to date [25], including Robert algorithm, Sobel algorithm, Canny algorithm, Hough transform algorithm [26-27]. The traditional Canny edge algorithm is robust, but does not readily provide the optimal threshold. Other researchers have attempted to improve the Canny algorithm, for example, by building a fast-adaptive threshold-based Canny algorithm or fusion vector machine-based Canny algorithm [28]. The Hough circle detection algorithm allows the user to detect multi circles quickly by positioning the radius and the centers of the circles [29-30]. These algorithms provide the basis for the extraction and calculation of surfaces. For the purposes of actual measurement, convex deformation size is unknown – it is simply a 3D surface distributed on the surface of the circular steel tube. Visual detection is highly subject to noise effects including surface welding spot traces in the tube and variation in illumination of the surrounding environment which altogether make image recognition and edge detection very difficult.

In this study, we developed a convex deformation calculation and edge image measurement technique based on monocular vision and laser rangefinder technology. The vision measurement system was built around the laser rangefinder through which a spatial-geometric relation is established between the laser, a camera, and the convex deformation. The image information of the convex deformation is obtained by the vision system, and then a fast optimization threshold-based improved Canny algorithm can be used to extract the edge of the curve. After removing a small amount of residual noise using dual gray values, the convex deformation parameters can be calculated via the circle Hough transform algorithm. Finally, the image detection system runs in OpenCV software and yields an automatic visual inspection.

2. Experimental setup

The diameter of the steel columns is 200mm, their length is 1600 mm, and the replacement rate of recycled concrete is 50%. The serial number of the specimens is as follows: H refers to the thick wall steel column (8 mm). B refers to the thin wall steel column (6 mm). D refers to the low-strength steel column (Q235). G refers to the high-strength steel column (Q345), and 1, 2, and 3 represent the axial compression ratio of the steel column (0.2, 0.4 and 0.6, respectively). The fourth number is the sample number. As shown in Fig.1.

We use a MTS pseudo dynamic testing system as a loading device for the columns and for vibration tests. As shown in Fig.2.

The test device was consisted of a controller and displacement sensors. The loading procedure described in the 'Regulations for seismic test of buildings' (JGJ 101-96) was employed. The loading method controlled by mixing the loading and displacement was applied in two stages. A loading gradation procedure with a capacity of 5 kN for every step was adopted until the specimens reached the yield loading capacity P_y, and every loading step had three circulations. After the specimens yielded, loading was controlled by the displacement method as an integral multiple of the yield displacement Δ_y. The loading procedure was terminated after obvious damage was detected or the loading capacity decreased to 85% of the ultimate capacity.

The artificial contact measurement environment included: an electronic digital calliper (300 mm range, accuracy of 0.01 mm) utilized to measure the maximum diameter of RACSC convex deformation, the distance between convex deformation and the base plane, and the diameter of the column.

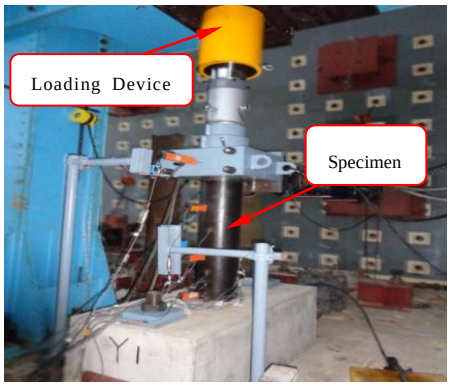

Fig. 1Testing environment

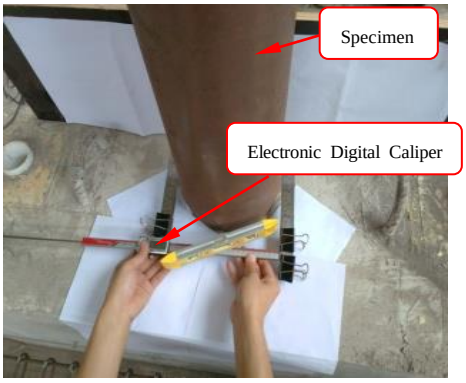

Fig.2 Artificial measurement

3. Monocular Vision-based Measuring Method

3.1. Measurement Principle

As shown in Fig.3, the proposed vision measurement system includes a digital video camera (model MV-VD120SC), colour video image acquisition card, tripod, calibration board, laser range finder (accuracy of 0.1 mm), computer and developed image detection software by our team. A flowchart of the RACSC convex deformation image detection system is provided in Fig.4.

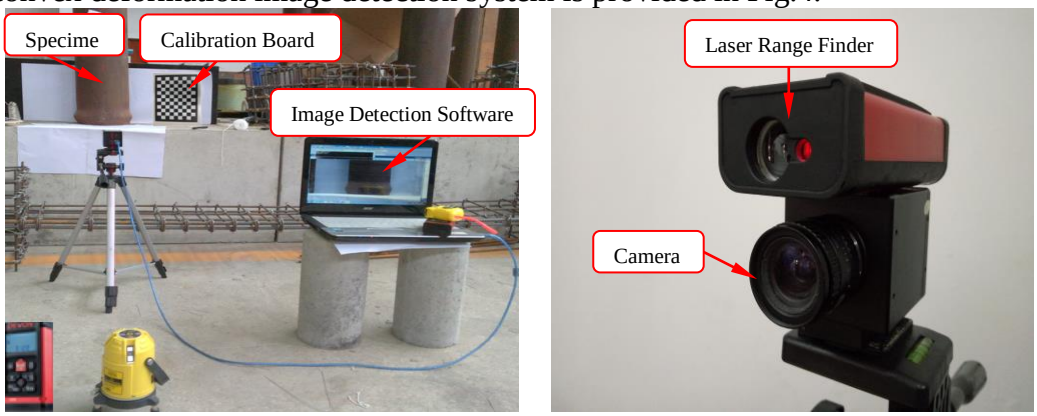

(a) Vision measurement system; (b) Single camera and the laser range finder

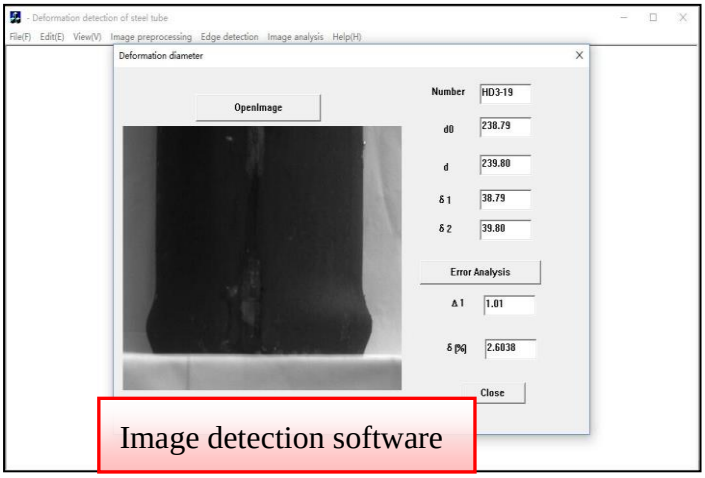

(c)Image detection software

Fig. 3 The proposed measurement system

The detection process includes camera calibration [31-32], image pre-processing, edge detection and parameter acquisition. The camera was calibrated using the plane target calibration method to determine its camera's focal length and distortion parameters [33], and other necessary information [34], based on which the acquired image can be corrected as necessary. Pixel

calibration yields the mapping relationship between the pixels in the image and the target parameters. The angle of monocular vision is less than 180 degrees, so it was necessary to establish a spatial-geometric relation between the camera and the target so that the RACSC convex deformation parameters could be indirectly calculated appropriately. The setup's range of view, Φ=2*r is shown in Fig.5.

The line of visual sight is tangent with the circle of the projection of the column. The tangent point is Q, and the maximum radius of convex deformation is perpendicular to the tangent line. The reference plane (datum plane), is assumed an auxiliary imaging plane that can be set in x-y form as the camera calibration datum (Fig.3a).

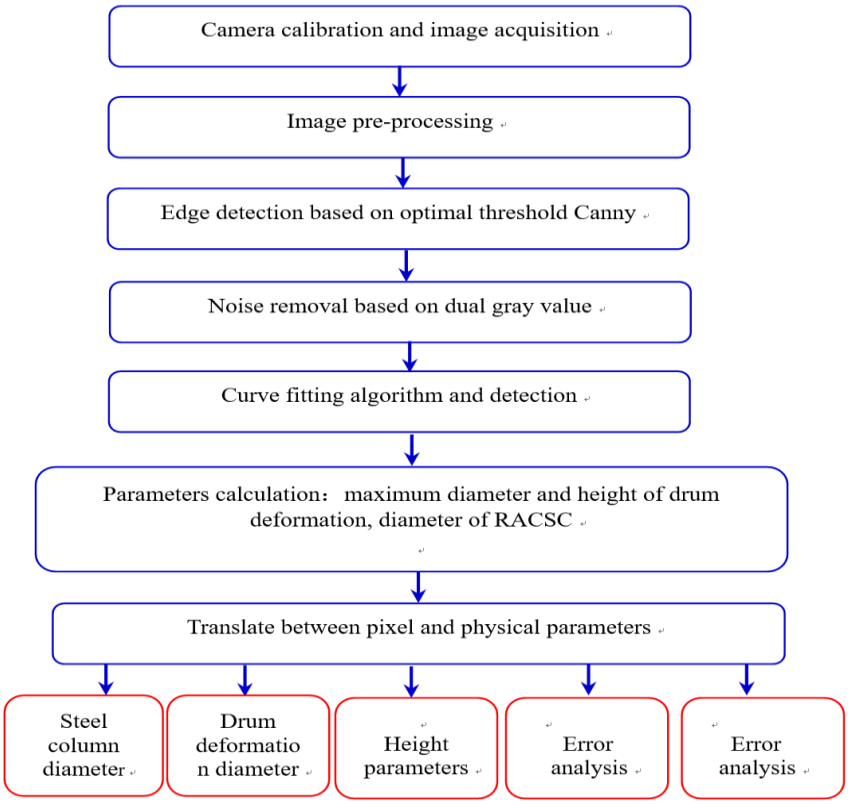

Fig. 4 Image detection flow

The depth direction from the camera to the target is z, the maximum projection diameter of the target image on the datum plane is d_1, the radius is r_1, the height is h_1, the maximum diameter of the convex deformation of the actual target image is d, and the radius is r. The difference between the projection and the actual target, ξ is calculated as follows:

$$\xi = \left|2r_1 - 2r\right| \tag{1}$$

The distance between the camera and the target detected is l_1, the height of the convex deformation is defined as h_0, the distance between the camera and the imaging plane is l, and the distance between the camera and the tangent point is defined as l_0, then r can be calculated as follows:

$$r = \frac{\left|l_0 r_1\right|}{l} \tag{2}$$

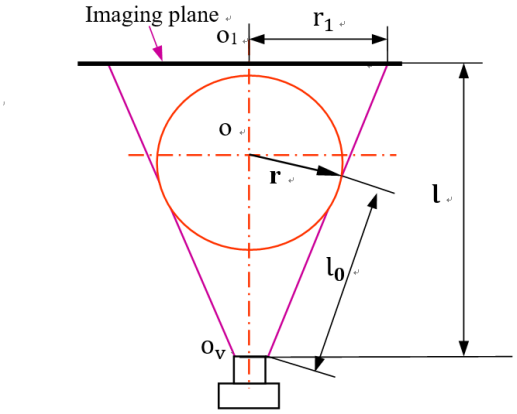

Fig. 5 Spatial geometric relation module

The width of the standard board is v (mm), the pixel width of the standard board is v_1 (mm), the pixel width of the maximum convex deformation place v_2 (mm), and the height of the convex deformation is h. Then, the following conversion formulas can be derived:

$$\frac{v_2}{2r_1} = \frac{v_1}{v} \tag{3}$$

$$\frac{h}{h_1} = \frac{v_1}{v} \tag{4}$$

From Eqs. (2) - (4) can be drawn to the following formula:

$$r = \frac{l_0}{2v_1 l} v_2 v \tag{5}$$

By this way, radius r can be obtained, while its unit is mm.

3.2. Calculating the convex deformation parameters

The bottom deformation areas of our test samples were detected using the proposed vision system to obtain 21 images of the cylinder and plane. The detection error was small when the distance between the camera and the target was in the

appropriate range, based on our laboratory calibration parameter tests, the appropriate distance between the camera and the target was 860 mm [34].

3.2.1 Fast optimal threshold-based Canny: Threshold selection affects image segmentation results. The traditional algorithm used for this purpose does not efficiently yield high and low thresholds, therefore the segmentation is not ideal, and i.e., excessive time (about one second) and memory are consumed for reselection. The same threshold may not be optimal for different environments and image edge characteristics. This section presents a novel fast optimization threshold technique that improves upon the traditional Canny algorithm to efficiently and accurately obtain image segmentation results. The proposed fast optimal threshold-based Canny algorithm works in the following steps.

Pre-process the RACSC and convex deformation images, and translate the colour to gray scale using the following RGB weighted average expression:

$$f(i,j) = 0.3R(i,j) + 0.59G(i,j) + 0.11B(i,j) \tag{6}$$

Where, R,G and B represent the three-primary colors ---Red, Green and Blue. All colors are obtained by mixing R, G, and B in different proportions.

Use the Gauss function to process the detection area and smooth the RACSC image and convex deformation edge image. Suppose that the image is $f(x,y)$, and the first derivative of two-dimensional Gauss's function is used to smooth the image; its function is as follows:

$$g(x) = \frac{1}{\sqrt{2\pi\sigma}} \exp(-\frac{(x-\mu)^2}{2\sigma^2}) \tag{7}$$

Where μ is the expected value of the Gauss distribution, x/y are the image coordinates, and σ is the standard deviation that controls the degree of smoothing.

The fast optimization threshold sets high and low threshold value as the combination of two variables, then variable operation instruction and the combination slide bar of high and low threshold values can be designed accordingly. For visualization, exploratory techniques can be used to quickly select the optimal combination threshold.

Use VC++ 7 and OpenCV to realize the above function, and develop a human-computer interaction-based threshold optimization image filter for detecting the convex deformation edge and removing noise (Fig. 6).

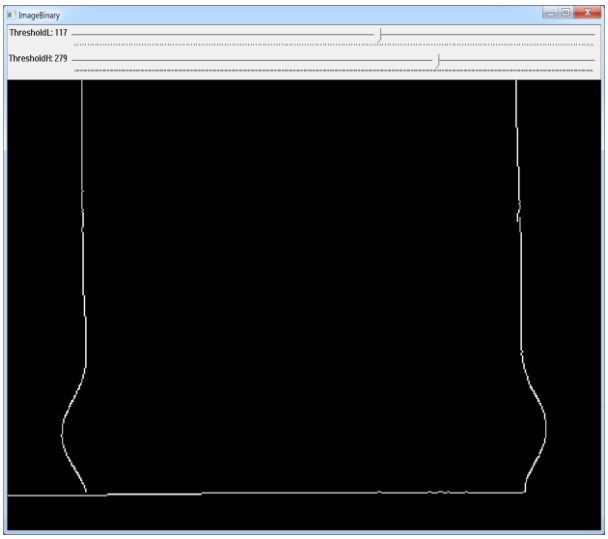

Fig. 6 Image filter base on fast optimal threshold

3.2.2 Dual gray value-based calculation of curve parameters： As shown in Fig. 6, the Hough circle transform effectively detected a continuous arc, however, the algorithm returned errors and ran slowly when there was even a small amount of noise. We established a dual-gray-value based Hough circle transform curve detection technique to remedy this. The Hough transform is utilized to detect the left and right contours (for example, lines,) then the gray values of all pixels (excluding edge points) in the region of the two contours are assigned to 0. The all-white interval is changed into black to reduce the residual noise, and then the following algorithm can be used to solve the tangent point coordinate:

Place each pixel of the image as the centre of a circle and draw a circle with known radius in the parameter plane. The results are accumulated then space image edge points can be mapped into the parameter space.

(1) Obtain an accumulated unit $M^{\mu}(x, y, r_{\mu})$.

(2) Find the peak point of the parameter plane $M_j^{\mu}(x_j, y_j, r_{\mu})$ with a position corresponding to the circle centre M.

(3) Sort $M_j^{\mu}(x_j, y_j, r_{\mu})$ by size. If there are N pixel points, the corresponding N accumulation units M_n^{μ}, M_{n-1}^{μ}, M_{n-2}^{μ} should be sorted to find the maximum value $M_{\max}^{\mu}$. Compare the first few accumulation units to determine the maximum tangent point.

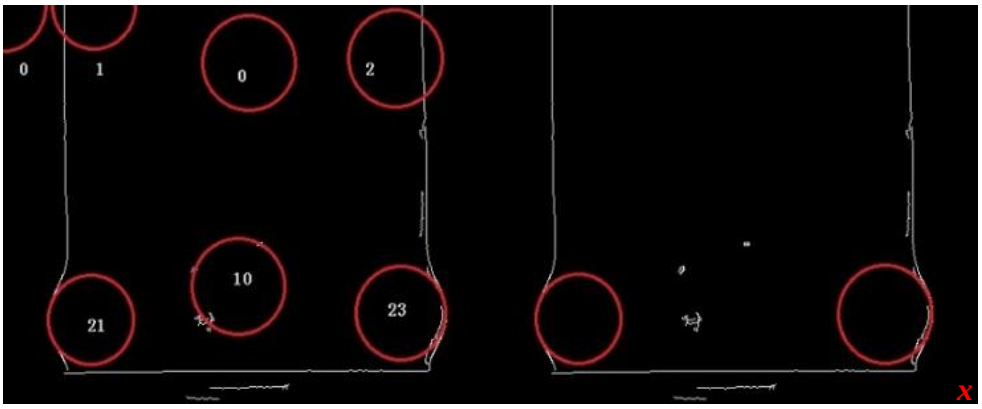

(a) Circle detection result (b) Tangent point detection result

Fig. 7 Traditional Hough circle transform result

3.2.3 Calculating tangent point pixel coordinates and parameters

Once the tangent point has been detected, the maximum convex deformation diameter pixel coordinates can be calculated through the point of tangency as follows: If the circle centre and radius of the circle tangent to convex deformation are known, the circle centre and radius of the i-th circle are x_i and r_μ, respectively and the coordinates of the tangent point $Q_i^\mu(x_i, y_i)$ can be calculated. Similarly, the pixel coordinates of the maximum convex deformation tangent point $Q_j^\mu(x_j, y_j)$ can be calculated. The diameter and height parameters can be obtained at the maximum convex deformation by pixel unit conversion.

4. Experimental Results

4.1 Performance of Fast Optimal Threshold-based Canny Algorithm

Fig.8 shows a comparison among four groups of typical threshold segmentations. The time consumption of the improved Canny algorithm edge detection was short (about 0.1 seconds), and the optimization effect was better than the artificial selection effect, in terms of low noise and high efficiency. There was still a small amount of noise in the BD3-9 and BG3-21 (Fig. 8d-f and Fig. 8j-l) fast optimization results, because the light was not uniform. This noise was fairly negligible, but did influence the maximum convex deformation profile parameters and calculation efficiency.

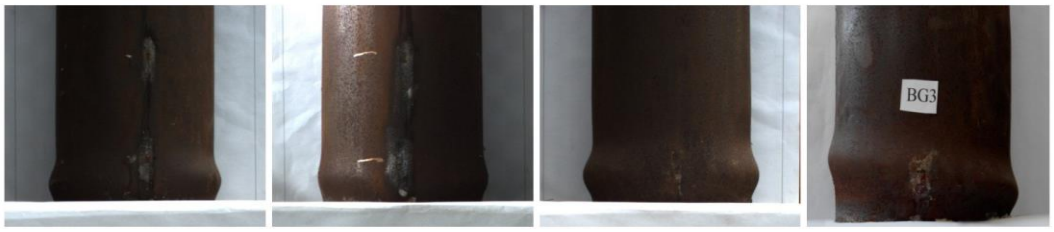

a）Original image of BD1-2, BD3-9, HD1-13, and BG3-21

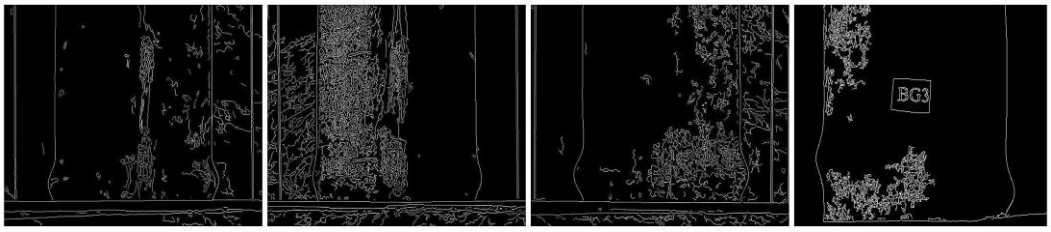

(b)Traditional Canny results of BD1-2, BD3-9,HD1-13, and BG3-21

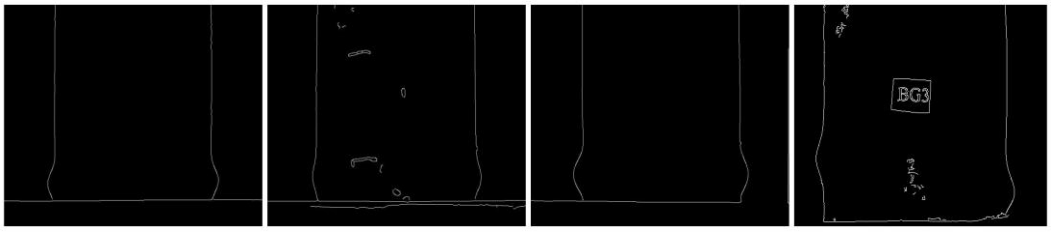

(c)Improved Canny results ofBD1-2, BD3-9, HD1-13, and BG3-21

Fig. 8 Comparison between improved algorithm and traditional algorithm
(a) Original images of BD1-2, BD3-9, HD1-13, and BG3-21;(b) traditional Canny results of (a); (c) Improved Canny results of (a).

4.2 Performance of Dual Gray Value Technique

As shown in Fig. 9a, the proposed algorithm outperformed the traditional Hough transformation (Fig. 7). The dual gray value technique removed a small amount of noise, thus improving the error identification in Hough circle transformation. The tangent point of the fitting circle and convex deformation was more accurate, as well, as shown in Fig. 9b.

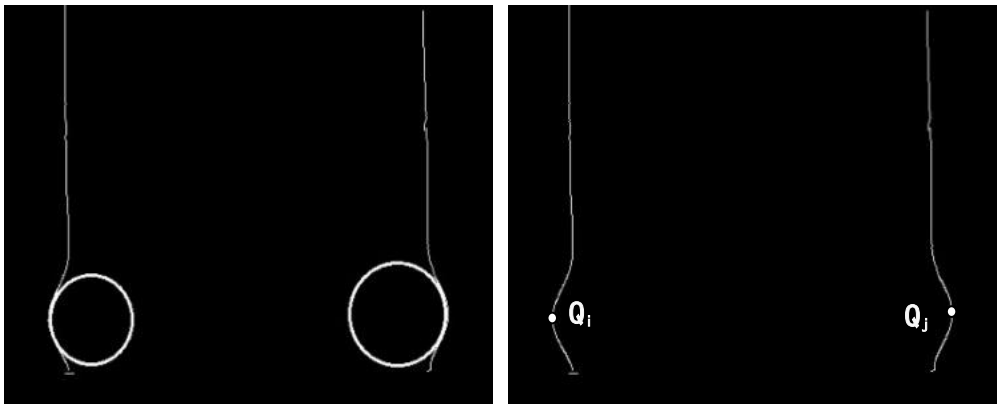

(a) (b)

Fig. 9 Proposed algorithm (a) Circle detection results; (b) Tangent point detection results

4.3 Detection Accuracy and Error Analysis

We used absolute error and relative error to measure the convex deformation diameter. The initial diameter of RACSC is D_0, artificial measured maximum convex deformation diameter is d_0, convex deformation is δ_1, and uniform linear increase in diameter is d_v. The maximum convex deformation diameter of image detection is d, convex deformation is δ_2, absolute error is Δ_1, and relative error is δ. See the following:

$$\delta_1 = d_0 \tag{8}$$

$$\delta_2 = d \tag{9}$$

$$\Delta_1 = \|d_0 - d\| = \|\delta_1 - \delta_2\| \tag{10}$$

$$\delta = \frac{\|\delta_1 - \delta_2\|}{\delta_1} \tag{11}$$

Table 1 presents the comparative data and error calculation results of the 21 groups of visual and manual tests.

In these 21 groups of convex deformation samples, 19 groups of errors fell between 0.06-0.99 mm accounting for 90.48% of the total. Group 1 (BD3-9) had error of 2.48 mm, accounting for about 4.76%. Because the diameter of RACSC has free - tolerance, the precision is usually between IT12-18. Thus, the maximum diameter of convex deformation by image detection was within a reasonable range. We also confirmed that the accuracy of our image detection technique was acceptable by comparison between the two methods.

Table1

Dimensions of deformation and damage assessment

Number	d_0 **(mm)**	d **(mm)**	δ_1 **(mm)**	δ_2 **(mm)**	Δ_1 **(mm)**	δ **(%)**	d_v **(mm)**
BD1-1	222.47	222.58	22.47	22.58	0.11	0.4888	208.46
BD1-2	220.94	221.57	20.94	21.57	0.63	2.9898	207.11
BD1-3	221.27	221.47	21.27	21.47	0.20	0.9403	208.21
BD2-4	214.49	214.29	14.49	14.29	0.20	1.4115	207.75
BD2-5	214.85	214.79	14.85	14.79	0.06	0.3844	208.28
BD2-6	215.64	215.73	15.64	15.73	0.09	0.5859	209.51
BD3-7	216.72	217.45	16.72	17.45	0.73	4.3727	208.68
BD3-8	218.55	217.81	18.55	17.81	0.74	3.9892	209.20
BD3-9	213.87	216.35	13.87	16.35	2.48	17.8808	208.10
BD3-10	216.87	216.81	16.87	16.81	0.06	0.3509	208.72
BD3-11	216.91	217.45	16.91	17.45	0.54	3.1780	209.11
BD3-12	216.6	217.31	16.6	17.31	0.71	4.2518	208.66
HD1-13	226.83	226.68	26.83	26.68	0.15	0.5518	208.48
HD1-14	226.20	225.94	26.2	25.94	0.26	0.9765	208.28
HD1-15	226.86	226.50	26.86	26.50	0.36	1.3426	208.68
HD2-16	216.41	217.11	16.41	17.11	0.70	4.2357	208.70
HD2-17	216.78	217.69	16.78	17.69	0.91	5.4297	208.82
HD2-18	227.00	226.01	27.00	26.01	0.99	3.667	208.84
HD3-19	238.79	239.80	38.79	39.80	1.01	2.6038	209.87
BG2-20	222.01	221.13	22.01	21.13	0.88	3.9982	209.02
BG3-21	233.12	233.95	33.12	33.95	0.83	2.5060	207.96
Average	221.10	221.35	21.10	21.35	0.60	3.1493	208.59

In summary, the image evaluation and analysis of RACSC damage deformation via the proposed method was effective. By analyzing the convex deformation maximum diameter, the distance from the base height, the convex deformation and the other necessary factors, the convex deformation of thin-walled and high-strength RACSCs was uneven, nonlinear local buckling deformation and the height of convex deformation was uneven and spiral in shape. The stress held by the thin-walled steel column is asymmetrical, so the deformation formed a spiral upon reloading. The height of convex deformation of

the thick-walled steel column was consistent, indicating that the deformation was symmetrical after loading. Our image analysis showed that after loading the diameters of other parts of the steel column linearly increased at an average value of 8.59 mm, while other parts of the steel column also produced deformation.

5. Conclusions

In this study, a novel image-processing algorithm of applicable to accessing the seismic damage of RACSCs was established and tested. The technique includes an image-detection method based on monocular vision and laser measurement of the surface of the convex deformation. The vision measurement system works based on a mathematical model of the spatial relationship among the camera, the laser range finder and the convex deformation. A fast optimization threshold method was designed as an improvement upon the traditional Canny algorithm for extracting the convex deformation edge information. A dual gray value method was introduced to remove a small amount of residual noise and convert the curve solution to find the tangent point of the curve and the fitting circle, thus simplifying the problem. Experimental results indicated that the optimization threshold effect of the proposed algorithm increased compared to the traditional algorithm. The de-noising ability of the proposed algorithm was higher than that of the traditional algorithm. The curve fitting with dual gray values to calculate convex deformation parameters had relatively smaller error, higher calculating efficiency, and is simpler in principle. The visual detection and image analysis of the deformation characteristics showed that convex deformation occurred at the bottom of RACSC. Further, the convex deformation of the thin-walled steel column was uneven and characterized by local deformation while that of the thick-walled steel column was symmetrical. Data from 21 groups of image detection tests showed that the average detection error of the proposed method was 0.6 mm, or 3.15%; in short, the proposed algorithm has reasonable accuracy, and thus can be readily applied to detecting the damage and deformation of RACSCs in practice.

Acknowledgments

This project was supported by a grant from the National Natural Science Foundation of China (No. 51578162, 11472084).

R E F E R E N C E S

[1]. *Yun-Chao Tang, Li-Juan Li, Wen-Xian Feng, Feng Liu, Bin Liao.* Seismic performance of recycled aggregate concrete–filled steel tube columns. Journal of Constructional Steel Research. (2017), 133, 112-24

[2]. *J.Valen; D. Dias-da-Costa; E.N.B.S. Júlio.* Characterisation of concrete cracking during laboratorial tests using image processing. Construction and Building Materials (2012), 28(1), 607–615.

[3]. *Yue Geng; Yu-Yin Wang; Jie Chen.* Time-dependent behaviour of steel tubular columns filled with recycled coarse aggregate concrete.Journal of Constructional Steel Research (2016), 122, 455–468.

[4]. *Wen-Xian Feng; Yun-Chao Tang; Ye Zhang et al.* Non-uniform Axial Force Precise Modelingand Simulation of Recycled Aggregate Concrete Confined by Steel Tube Column. Journal of System Simulation (2015), 27(2), 410-417.

[5]. *Christian Koch.; Kristina Georgieva.; Varun Kasireddy.* A review on computer vision based defect detection and condition assessment of concrete and asphalt civil infrastructure. Advanced Engineering Informatics (2015), 29(2), 196-210.

[6]. *Ashtiani, R.,Saeed, A.,Hammons, M.*. Mechanistic Characterization and Performance Evaluation of Recycled Aggregate Systems. J. Mater. Civ. Eng. (2014), 26, 99-106.

[7]. *Feng Liu.; Yin-Yin Yu.; Li-Juan Li.* A seismic performance analysis of recycled concrete filled circular steel tube columns. China Civil Engineering Journal (2013), 46(2), 178–184.

[8]. *You-Fu Yang.;Zhi-Cheng Zhang.* Tests on Circular Recycled Aggregate Concrete-filled Steel Tubular Members under Lateral Impact Loads. China Journal of Highway and Transport (2014).27(11), 32-38.

[9]. *Bo Wu; Xin-Yu Zhao;Jin-Suo Zhang.* Cyclic behavior of thin-walled square steel tubular columns filled with demolished concrete lumps and fresh concrete. Journal of Constructional Steel Research, (2012), 77, 69-81.

[10]. *Hui Ma; Jian-Yang Xue; Yun-He Liu; et al.* Cyclic loading tests and shear strength of steel reinforced recycled concrete short columns. Engineering Structures, (2015), 92 (1), 55-68.

[11]. *Vivian W.; Y. Tam.; Zhi-Bin Wang.; Zhong Tao*. Behaviour of recycled aggregate concrete filled stainless steel stub columns. Materials and Structures (2014), 47,293-310.

[12]. *Bensaid Boulekbache.; Mostefa Hamrat.; Mohamed Chemrouk.; et al.* Failure mechanism of fibre reinforced concrete under splitting test using digital image correlation. Materials and Structures (2015), 48(8), 2713–2726

[13]. *Jian-Zhuang Xiao.; Hong Li.; Jun-Qiang Yuan.* Application of Digital Image Technique in Behavior Analysis of Recycled Aggregate Concrete. Journal of Building Materials (**2014**), 17(3), 459–464.

[14]. *Bao-Hua Shan.; Shi-Jie Zheng.; Jin-Ping Ou.* A stereovision-based crack width detection approach for concrete surface assessment. KSCE Journal of Civil Engineering (**2016**), 20(2), 803–812.

[15]. *Jing Tong; Xian-yu Jin; Ye Tian et al.* Study on surface cracking of corroded reinforced concrete based on DIC method. Journal of Zhejiang University (Engineering Science). (**2015**).49(2), 193-199.

[16]. *R.S.Adhikari.; Moselhi, A.; Bagchi.* Image-based retrieval of concrete crack properties for bridge inspection. Automation in Construction (2014), 39(1), 180–194

[17]. *Dong-ming Feng; Maria Q.Feng; Ekin Ozer.* A Vision-Based Sensor for Noncontact StructuralDisplacement Measurement. Sensors (**2015**), 15, 16557-16575.

[18]. *Gang Li; Shuan-Hai He; Yong-Feng Ju; Kai Du.* Long-distance precision inspection method for bridge cracks with image processing. Automation in Construction (**2014**), 41(5), 83–95

[19]. *Belen Ferrer.; Pablo Acevedo.; Julian Espinosa.* Targetless image-based method for measuring displacements and strains on concrete surfaces with a consumer camera, Construction and Building Materials (2015), 75(30), 213–219

[20]. *Chun-Tang Chao; Ming-Hsuan Chung; Juing-ShianChiou; et al.* A Simple Interface for 3D Position Estimation of a Mobile Robot with Single Camera. Sensors (2016), 16(4), 435-1-12

[21]. *Xue-Jun Xu; Xiao-Ning Zhang*. Rapid Crack Detection of Concrete Bridges Based Digital Image. Journal of Hunan University (Natural Sciences) (2013), 40(7), 34–40

[22]. *Xue-Li Hao; Ai-Min Sha; Zhao-Yun Sun; Wei Li;Yan-ju Hu*. Laser-based measuring method for mean joint faulting value of concrete pavement. Optik. (2016), 127, 274–278.

[23]. *Savas Erdem.; Marva Angela Blankson*. Fractal–fracture analysis and characterization of impact-fractured surfacesin different types of concrete using digital image analysis and 3D nanomaplaser profilometery.Construction and Building Materials (2013),40,70–76.

[24]. *Abdel-Jaber, H.; Glisic, B.*. Analysis of the status of pre-release cracks in prestressed concrete structures using long-gauge sensors. Smart Mater. Struct. (2015), 24, doi:10.1088/0964-1726/24/2/025038

[25]. *Song Wang; Joachim S.; Stahl.;* Adam Bailey.;Michael Dropps.. Global Detection of Salient Convex Boundaries. International Journal of Computer Vision (2007), 71(3), 337–359.

[26]. *Mustafa Turker.; Dilek Koc-San.* Building extraction from high-resolution optical space borne images using the integration of support vector machine (SVM) classification, Hough transformation and perceptual grouping. International Journal of Applied Earth Observation and Geo information (2015),34(2) ,58–69.

[27]. *E. A. S. Galvanin.; G. M. do Vale; A. P. Dal Poz.* The canny detector with edge region focusing using an anisotropic diffusion process. Pattern Recognition and Image Analysis (2006), 16(4) , 614–621

[28]. *Zhen-Jun Tang; Li-Yan Huang; Xian-Quan Zhang; et al*. Robust image hashing based on color vector angle and Canny operator. AEU - International Journal of Electronics and Communications (**2016**),70,(6), 833–841.

[29]. *Anna Maria Massone.; Annalisa Perasso.; Cristina Campi.; et al*. Profile Detection in Medical and Astronomical Images by Means of the Hough Transform of Special Classes of Curves. Journal of Mathematical Imaging and Vision (2015), 51(2), 296–310.

[30]. *Ke Chen.; Jian-Ping Wu.; Jin-Xiang Li.; et al.*, Robust Real-Time Multi-Circle Detection Algorithm Based on 1D Probabilistic Hough Transform. Journal of Computer-Aided Design & Computer Graphics (2015), 27 (10), 1832–1841

[31]. *De-Feng Wu.; Tian-Fei Chen.; Ai-Guo Li.* A High Precision Approach to Calibrate a Structured Light Vision Sensor in a Robot-Based Three-Dimensional Measurement System. Sensors (2016), 16(9), 1388-1-18

[32]. *Bao-Hua Shan; Shi-Jie Zheng; Jin-Ping Ou*; Free vibration monitoring experiment of a stayed-cable model based on stereovision. Measurement (**2015**), 76, 228–239.

[33]. *Xiang-Jun Zou; Gui-Chao Lin; Yun-Chao Tang et al.* Sub-Pixel object-Image Registration Using Improved Iterative Closest Point Method. Journal of Computer-Aided Design & Computer Graphics.(**2016**),28(8),1242-1249.

[34]. *Xiang-Jun Zou; Hai-Xin Zou; Jun Lu*. Virtual manipulator-based binocular stereo vision positioning system and errors modeling. Machine Vision and Applications (2012), 23(1), 43–63.